UNIVERSITY OF CALIFORNIA SAN DIEGO

Colloidal Synthesis of the 2H and 2M Phases of Tungsten Disulfide Nanocrystals

A thesis submitted in partial satisfaction of the
Requirements for the degree Master of Science

in

Chemistry

by

Ashley Katelyn Tamura

Committee in charge:

Professor Alina Schimpf, Chair
Professor Clifford Kubiak
Professor Brian Leigh

2021

The thesis of Ashley Katelyn Tamura is approved, and it is acceptable in quality and form for publication on microfilm and electronically.

University of California San Diego

2021

EPIGRAPH

“It’s like you’re always stuck in second gear
When it hasn’t been your day, your week, your month, or even your year.

But, I’ll be there for you when the rain starts to pour.
I’ll be there for you, like I’ve been there before.
I’ll be there for you ‘cause you’re there for me too.”

- *Friends*

TABLE OF CONTENTS

LIST OF FIGURES

LIST OF TABLES

LIST OF ABBREVIATIONS

Bond dissociation energy	BDE
Chemical vapor deposition	CVD
Dodecanethiol	DDT
Field-effect transistor	FET
Hexamethyldisilazane	HMDS
Hydrogen evolution reaction	HER
Nanocrystal	NC
Oleic acid	OA
Reduced graphene oxide	RGO
Transition metal dichalcogenide	TMD
Trioctylphosphine oxide	TOPO
Two-dimensional	2D
X-ray diffraction	XRD

ACKNOWLEDGEMENTS

I would first like to thank Ricardo de Luna in the Sailor group for helping me get reliable access to their Raman spectroscopy instrument throughout the pandemic. Additionally, I would like to thank everyone in my research group for being there for me during this entire process. It has been a difficult past couple of years, not to mention the pandemic, so I am grateful to have had such a kind, supportive group of lab mates to help guide me to the finish line. In particular, I would like to thank Jessica Geisenhoff for mentoring me ever since I was an undergraduate student and always being so kind and supportive. Even when I made a mistake, she would find a way to put a positive spin on it and treat it as a valuable learning experience. I would also like to thank Alina Schimpf for honestly so much. For taking a chance on an overeager undergraduate student with minimal relevant experience, for humbly treating everyone she works with as equals, and for knowing how to push people in the direction they need to go without being too forceful. To everyone, thank you. I could not have done this without you.

Material from various chapters, namely Chapter 6, in part are currently being prepared for submission for publication. Ms. Tamura will be the third author on this paper. Geisenhoff, J. Q.*; Yin, H.*; Tamura, A. K.; Schimpf, A. M. Crystal-bound thiols for the interlayer expansion of tungsten and molybdenum disulfide nanocrystals. In preparation. *These authors contributed equally.

ABSTRACT OF THE THESIS

Colloidal Synthesis of 2H and 2M Phase Tungsten Disulfide Nanocrystals

by

Ashley Katelyn Tamura

Master of Science in Chemistry

University of California San Diego

Professor Alina Schimpf, Chair

Layered materials have recently gained a lot of attention, in particular group-VI transition metal dichalcogenides (TMDs). This class of materials exhibits unique phase-specific properties ranging in behavior from metallic to semiconducting to topologically insulating. Selecting for a single phase to utilize for their desired applications can be challenging, however, due to their similar ground state energies. Here we examine WS_2 nanocrystals (NCs), which nucleate as the metastable 2M phase and gradually convert to the thermodynamically-favored 2H phase. We develop a phase-tunable colloidal synthesis by controlling the reactivity to either hinder or promote rapid phase conversion

in order to access the 2M and 2H phases, respectively. We found that inclusion of oleic acid (OA) decreases the reactivity of the tungsten hexacarbonyl precursor, resulting in reduced phase-conversion upon reaction with sulfur. Reactivity of the W and S precursors can, however, be promoted by utilizing the one-pot method of sulfur addition, in which sulfur is present during the heating process. This increase in the direct W–S reactivity leads to rapid phase-conversion. Finally, we compare the reactivity of various S-precursors, including thiols and diorgano disulfides. The use of thiols results in more rapid phase-conversion, which we hypothesize is due to increased interlayer distances enabled by the incorporation of the alkyl group as a "crystal-bound" ligand. Collectively, these synthetic tools offer controllable access to either the 2M or 2H phase of WS_2 NCs.

Chapter 1: Introduction to Phase-tunable TMD Syntheses

Two-dimensional (2D) materials have gained a lot of research interest following the discovery of the diverse properties of graphene,[1] which is a monolayer of graphite. Unlike graphite, graphene has a high carrier mobility and can be utilized as an ultra-thin electrical and thermal conductor.[2-3] In general, 2D materials exhibit many layer-dependent properties that stem from their unique structure made up of one or more strong covalently bonded layers that exhibit weak interlayer bonding. In particular, group-VI transition metal dichalcogenides (TMDs) have been studied extensively due their crystal-phase-dependent properties, allowing them to exhibit behavior ranging from metallic to semiconductor to topological insulator.[4-7] Group-VI TMDs are a class of nanomaterials with the formula MX_2, where M = Mo, W and X = S, Se, Te. These materials form layered structures of the form X–M–X, with the chalcogen atoms in two hexagonal planes separated by a plane of metal atoms. The adjacent layers together form the bulk structure of each crystal-phase.

Group-VI TMD NCs come in several distinct crystal-phases that differ based on their monolayer structure type and the interlayer stacking order, which are shown in Figure 1. The three types of monolayer structure types are 1H, 1T, and 1T′. The 1H-type layer has trigonal prismatic coordination of the metal, while the 1T-type layer has octahedral coordination as well as inversion symmetry. Compared to the 1H-type layer, the 1T-type layer is typically higher in energy among group-VI TMDs,[8] rendering this structure type metastable. This causes the 1T-type layer to have intrinsic structural instability, making it prone to spontaneously relax to the more stable and energetically

favorable 1T′ structure, which also has inversion symmetry. This is known as a Peierls transition and is driven by electron-phonon interactions.[9] These three monolayer structure types (1H, 1T and 1T′) can stack in different ways in order to form the various crystal-phases. One crystal structure that we will be focusing on is the 2H phase ($P6_3/mmc$), which has two 1H-type layers per repeating unit and has hexagonal symmetry. The other known 1H stacking mode is the 3R phase ($R3m$), which has three 1H-type layers per repeating unit with rhombohedral symmetry. The 1T-type layer has just one stacking mode, which has tetragonal symmetry with one 1T-type layer per repeating unit. Three 1T′ stacking modes exist, one of which is the 1T′ phase ($P2_1/m$) and contains two 1T′-type layers per repeating unit. Recently, the 2M phase (C2/m) was discovered,[10] which is monoclinic and consists of two 1T′-type layers per repeating unit. The third 1T′ stacking mode is the orthorhombic T_d phase (Pnm21), in which inversion symmetry is broken.

A quick thing to note when referencing the literature is that the metastable 2M phase of tungsten disulfide was not discovered until recently.[10] Prior to that, it was understood that the monolayers of the metastable phase were 1T′-type, but the stacking order was mistakenly thought to be the same as the 1T′ phase. Because of this, the 2M phase of tungsten disulfide was commonly referred to in the literature as the 1T′ phase. It is now understood that the metastable phase of tungsten disulfide is in fact the 2M phase, not 1T′.

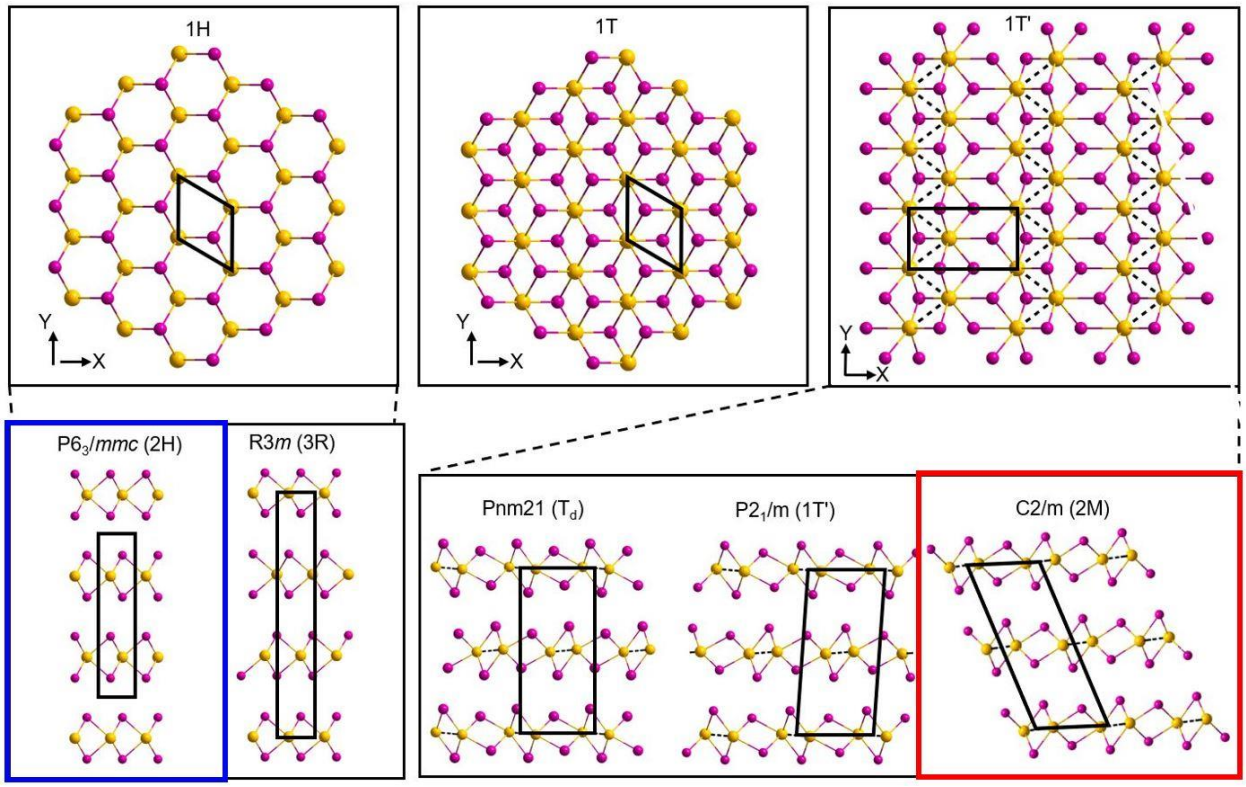

Figure 1: Crystal-phases of group-VI TMD NCs. Group VI transition metal atoms (M = Mo, W) are yellow, and chalcogen atoms (X = S, Se, Te) are pink.

Each crystal-phase of group-VI TMDs has its own distinct properties and applications. The T_d phase, for example, is a polymorph of bulk molybdenum ditelluride and tungsten ditelluride studied for its unique semi-metallic properties. On the other hand, the 3R phase is semiconducting with promising applications in spintronic devices.[11] Its challenging direct synthesis, however, has only been reported through chemical vapor transport methods.[11-12] Here we primarily discuss the 1T, 2H and 2M phases, since these are the known available phases of tungsten disulfide that have the potential to be synthetically tuned, the methods of which will be discussed in the next section. To begin, the 2H phase is semiconducting and thus has applications in optoelectronics[7] due to its direct band gap in the monolayer. In addition to their structural stability and high carrier mobility, these materials are particularly attractive to use as field-effect transistors (FETs)

in electronic devices[5, 7, 13] as well as in combination with graphene due to their synergistically enhanced on/off ratios and larger on current.[14] On the other hand, the 1T phase is metallic, making it useful in applications in catalysis.[6] For example, the 1T phase of WS_2 as well as MoS_2 have been widely studied for their potential in hydrogen evolution reaction (HER) catalysis due to the active edge sites of their nanosheets and their stability against photocorrosion compared to commonly used materials such as CdS.[15-18] The loosely stacked layers of TMDs also help accommodate some structural changes along the z-axis, promoting structural stability in hybrid materials, such as WS_2 on reduced graphene oxide (RGO)[19] and also MoS_2 on RGO,[20] in addition to enhanced catalytic properties. As mentioned, the 1T phase of group-VI TMDs often undergoes a spontaneous transition to the 1T′ phase. This has been theoretically determined to be a topological phase transition,[21] allowing conducting edge sites to exist in an otherwise insulating material. This topological insulator behavior arising in the 1T′ phase of group-VI TMDs allows potential applications in spintronic devices due to their spin and valley coupling at the monolayer level.[22-23] In order to utilize the phase-specific properties in these materials for their desired applications, a synthetic scheme offering precise control over thickness, crystal-phase and surface chemistry must first be developed.

Intensive studies have been done to develop efficient and controllable methods for producing NCs, some of which offer the structural tunability desired for developing phase-tunable syntheses of TMDs. Two main categories exist for synthesizing these materials, being top-down and bottom-up approaches. The top-down approach typically involves using external forces to break apart a bulk crystal or to exfoliate nanosheets into smaller segments, allowing large batches of monolayers to be processed. This approach,

however, offers little control over structural properties, making it unsuitable for our purposes. On the other hand, the bottom-up approach involves the chemical reaction of elemental precursors or other building blocks coming together to form NCs. One bottom-up method commonly used for TMD synthesis is chemical vapor deposition (CVD),[6, 24-25] where the metal precursor bound to a substrate reacts with a chalcogen precursor at high temperatures while using little to no solvent. This enables the production of large TMD monolayers free of surface ligands, but offers limited homogeneity and currently lacks control over morphology. An alternative method to preparing TMDs is colloidal synthesis, [24-26] which typically involves the chalcogen and transition metal precursors being heated at moderate to high temperatures in an organic solvent. At this point, the chalcogen and metal precursors decompose to form monomers followed by rapid nucleation upon reaching a critical concentration minimum, after which they grow by diffusion to form NCs.[27] The colloidal synthesis method benefits from its ability to utilize ligands to cap and effectively passivate growth off of specific facets of the NC during synthesis, promoting phase tunability.[24] Additionally, altering synthetic parameters, such as choice of ligand, precursors, and growth time, offers tunability over size, shape, and phase.[4, 24-26, 28-37] Overall, this method offers us the highest potential for tuning the crystal phase of synthesized TMD NCs, which ultimately allows control over their phase-specific electronic properties.

Several methods exist for tuning the crystal-phase of colloidally synthesized metal chalcogenide-based NCs, one of which involves selecting a chalcogen precursor based on its reactivity. In the case of organosulfur precursors, one factor that can determine reactivity has to do with the C–S bond strength. Thus, Rhodes et al. found that using

sulfur precursors with a low bond dissociation energy (BDE) resulted in an increased reactivity of sulfur, which promoted formation of sulfur-rich phases of iron sulfide NCs.[28] Likewise, using sulfur precursors with a high BDE promoted formation of sulfur-deficient phases. While choosing an appropriate chalcogen precursor can be useful, this method can be limited based on the number of possible chalcogen precursors available. To bypass this, ligands have been employed to controllably tune the reactivity of a given chalcogen precursor. For example, using a ligand capable of interacting with the chalcogen can effectively alter its reactivity in the process. This has been shown with the colloidal synthesis of nickel sulfide NCs, where 1-dodecanethiol (DDT) was suggested to have either formed complexes with monomers of the decomposed sulfur precursor or bound to the surface of the growing NCs.[30] This led to slower diffusion and incorporation of the sulfur into growing NCs, resulting in the formation of more sulfur-deficient crystal-phases as the amount of DDT added was increased. Another method worth mentioning includes the use of a reducing agent, which has been used to alter the reactivity of a chalcogen precursor by changing its speciation during colloidal NC synthesis, subsequently offering phase tunability.[33]

Ligands have also been employed to tune the phase of NCs based on their ability to interact with metals. One example involves the use of ligands to mediate topotactic phase conversion in colloidal NCs. In the case of $AgInSe_2$, this is attributed to the ligand cation-exchange mediators, being oleylamine or 1-dodecanethiol ligands, assisting in the extraction of Ag^+ ions from the structure of Ag_2Se. This is necessary for In^{3+} ion-diffusion, which promotes conversion to the metastable phase.[31] Other examples include the preferential coordination of ligands with a metal precursor during synthesis, which can

alter its reactivity and subsequently the rate of reaction. This has the potential to alter formation of a given crystal-phase as well. Such is the case with colloidally synthesized cesium lead bromide perovskite NCs, where alkyl-amines and alkyl-acids are believed to bind to Br and Pb atoms of the NC, respectively.[29] These interactions are thought to play a role in how excess oleylamine and oleic acid are able to promote Cs-rich and Pb-rich synthetic conditions, respectively.[34] The choice and ratio of solvents can then be manipulated to tune the phase of cesium lead bromide NCs, as their crystal-phases are highly dependent on composition. Similar results have been shown in the syntheses of tungsten diselenide NCs, where OA and oleylamine ligands have been suspected to coordinate with the tungsten hexacarbonyl metal precursor.[32, 35] This leads to slower reactivity and offers control over the formation of the kinetically and thermodynamically favored phases.

Utilizing ligands to tune the reactivity of the metal precursor has also been key in developing phase-tunable colloidal syntheses for WS_2 NCs. For example, Mahler et al. were able to tune the 2H and 2M phases of tungsten disulfide based on the inclusion of hexamethyldisilazane (HMDS) to the reaction mixture.[36] Specifically, they suspect that OA present during synthesis is capable of coordinating with tungsten, which causes a reduction in its reactivity and promotes formation of the metastable 2M phase. Thus, upon addition of HMDS, which likely complexes with OA to prevent it from accessing tungsten, the thermodynamically favored 2H phase is formed. Similarly, Liu et al. achieved phase-tunability based on the inclusion of either oleic acid or oleylamine as part of the organic solvent mixture.[37] They attributed the differences in phase-conversion, however, to the ability of oleylamine to stabilize the metastable 2M phase based on electrostatic

interactions. However, it likely has more to do with the interactions between the oleic acid/oleylamine and tungsten precursor altering the reactivity and subsequently tuning the phase.

Here we develop a phase-tunable colloidal synthesis for WS_2 NCs by utilizing OA, thiol, and the method of sulfur addition to tune the rate of conversion from the 2M to 2H phase by altering the tungsten precursor reactivity and promoting lattice expansion. We begin by demonstrating that WS_2 NCs must first nucleate as the 2M phase, followed by gradual conversion to the 2H phase over time. This indicates a link between the overall reaction rate and the rate of phase conversion, given that increased reactivity would promote increased phase conversion and vice versa. We then focus on oleic acid (OA) which we suggest may be forming a trinuclear tungsten species with tungsten hexacarbonyl, which has a comparatively lower reactivity, resulting in a decrease in phase conversion. The formation of this trinuclear tungsten species was also found to be tunable based on the sulfur addition method. This gives control over whether the more or less reactive tungsten species is predominantly present to react with sulfur precursor, offering further tunability over phase-conversion via reactivity. Finally, we propose that thiols, can be used to increase the rate of phase conversion by embedding themselves into the crystal lattice during synthesis. Their bulky, intact R groups then work to expand the interlayer distance, which effectively opens up space for further rearrangement and ultimately promotes rapid phase conversion from the 2M to the 2H phase.

Chapter 2: Materials and Experimental Methods

All chemicals used as received without further purification.

Table 1: Chemical Reagents. Chemical name, purity, and manufacturer shown for all chemicals used.

Chemical Name	Purity	Manufacturer
Tungsten hexacarbonyl	99%	Acros Organics
1-Dodecanethiol	98%	Acros Organics
1-Octanethiol	97%	Acros Organics
Diallyl disulfide	80%	Alfa Aesar
Dibenzyl disulfide	98%	Alfa Aesar
Diphenyl disulfide	98%	Alfa Aesar
Methanol	99.5%	Fisher Chemical
Toluene	99.5%	Fisher Chemical
Oleic acid	97%	Fisher Science Education
Trioctylphosphine oxide	90%	Strem Chemicals
n-Octyl Sulfide	97%	Tokyo Chemical Industry

In a typical synthesis using the hot-injection method, a 50-ml three-neck round bottom flask containing a glass stir bar, air condenser, and flow adaptor were first cleaned in a base bath, rinsed, and dried in an oven at 100°C. They were then connected with vacuum grease, attached to a Schlenk line under nitrogen, and placed on a heating mantle on a stir plate. The oleic acid and TOPO were then added to the flask. A thermocouple protected by a glass sheath was added to one neck, and the other neck was capped with a rubber septum. The flask was then heated to 110°C and put under vacuum for 1-2 hours. The reaction setup was then detached from the Schlenk line and put in a nitrogen-filled glovebox, where the tungsten precursor was then added to the flask. At the same time, a 25-mL three-neck round bottom flask containing 1.0 mL of TOPO and a stir bar connected with a flow adaptor was cleaned and degassed in a similar manner and brought into the glovebox, where the sulfur precursor was then added to the

flask. This stock solution and the main reaction setup were then reattached to the Schlenk line under nitrogen. The reaction setup was then heated to the desired reaction temperature, while the stock solution was warmed to around 80°C. Upon reaching the target temperature, 1.0 mL of the stock solution was injected into the main reaction flask. The reaction then proceeded for the desired reaction time. Afterward the heating mantle was removed, and the reaction flask was allowed to cool to ambient temperature. The reaction flask was then opened to air and added to test tubes. Some methanol was added, and then the solution was centrifuged at 3600 rpm. The supernatant was decanted, and the NCs were then washed twice by redispersing in 2:1 toluene/methanol and centrifuging at 3600 rpm to collect precipitated NCs. Finally, the particles were redispersed in toluene and used to prep Raman and samples for analysis.

The one-pot method is similar except that instead of having a stock solution of the sulfur precursor that was injected into the reaction flask, the sulfur precursor is added to the flask along with the tungsten precursor prior to heating. Reaction time began being counted once the reaction flask was heated to the desired reaction temperature. Table 2 indicates amounts of reagents used for the syntheses of 0, 2, and 100 eq of OA to $W(CO)_6$, and Table 3 indicates amounts of reagents used for the syntheses of various ratios of moles of sulfur precursor to moles of $W(CO)_6$.

Table 2: Reagent table for OA eq reactions. Amounts of reagents used for the 0, 2, and 100 eq of OA to $W(CO)_6$ reactions.

	S precursor	$W(CO)_6$	Oleic Acid	TOPO
0 eq	0.20 mmol	0.060 mmol	0 mmol	56 mmol
2 eq	0.20 mmol	0.060 mmol	0.12 mmol	56 mmol
100 eq	0.20 mmol	0.060 mmol	6.0 mmol	50. mmol

Table 3: Reagent table for sulfur ratio reactions. Amounts of reagents used for the reactions of various ratios of sulfur to $W(CO)_6$.

	S precursor	$W(CO)_6$	Oleic Acid	TOPO
2:1 S/W	0.12 mmol	0.060 mmol	0 mmol	56 mmol
3:1 S/W	0.18 mmol	0.060 mmol	0 mmol	56 mmol
4:1 S/W	0.24 mmol	0.060 mmol	0 mmol	56 mmol
6:1 S/W	0.36 mmol	0.060 mmol	0 mmol	56 mmol

Chapter 3: Phase-conversion over Time

In colloidal syntheses, one parameter commonly used to tune NC properties, such as crystal phase, involves tuning the reactivity. This is significant in cases like with nickel sulfide, where altering the reactivity and mobility of the sulfur promotes either sulfur-rich or sulfur-deficient crystal phases to form.[30] This is the result of more reactive and mobile sulfurs being easier to incorporate into growing NCs and thus increase the total number of sulfurs per NC in cases where crystal phases are dependent on composition. Here, we show that WS_2 NCs exhibit phase change from the metastable 2M to the thermodynamically favored 2H phase over time. Thus, altering the reactivity is significant as it can lead to more rapid phase-conversion to achieve the 2H phase or stunt the reaction to prevent phase-conversion, resulting in primarily the metastable 2M phase. The remaining chapters will go in more depth on how to tune phase-conversion by altering the reactivity in some way.

Throughout, we primarily utilize Raman spectroscopy in the following experiments to distinguish the phase of the crystal structure. The 2H phase of tungsten disulfide nanocrystals exhibits distinct peaks by Raman at approximately 354 and 416 cm^{-1} associated with the E_{2g} and A_{1g} modes respectively, while the bulk 2M phase of tungsten disulfide was recently found to have characteristic peaks at approximately 304 and 407 cm^{-1}. By comparing the intensity of the peaks in the Raman spectra, the 2H and 2M phases can then be distinguished to determine the relative amounts of each phase in a given sample.

Phase-conversion of our material can then be demonstrated by analyzing the Raman spectra for timed aliquots from a typical reaction. In Figure 2a, Raman peaks characteristic of 2M phase WS_2 can be seen when the reaction mixture first reached the target temperature and up to 10 minutes into the reaction. A mixture of 2H and 2M phase Raman peaks are present by 30 minutes. By the end of the reaction, the Raman spectrum is dominated by 2H phase. To better visualize the phase-conversion in the Raman spectra, Figure 2b is shown to illustrate the intensity ratios of the 2H/2M peaks with respect to time. The 2H peak associated with the intensity peak at 354 cm^{-1} and the 2M peak associated with the intensity peak at 304 cm^{-1}.

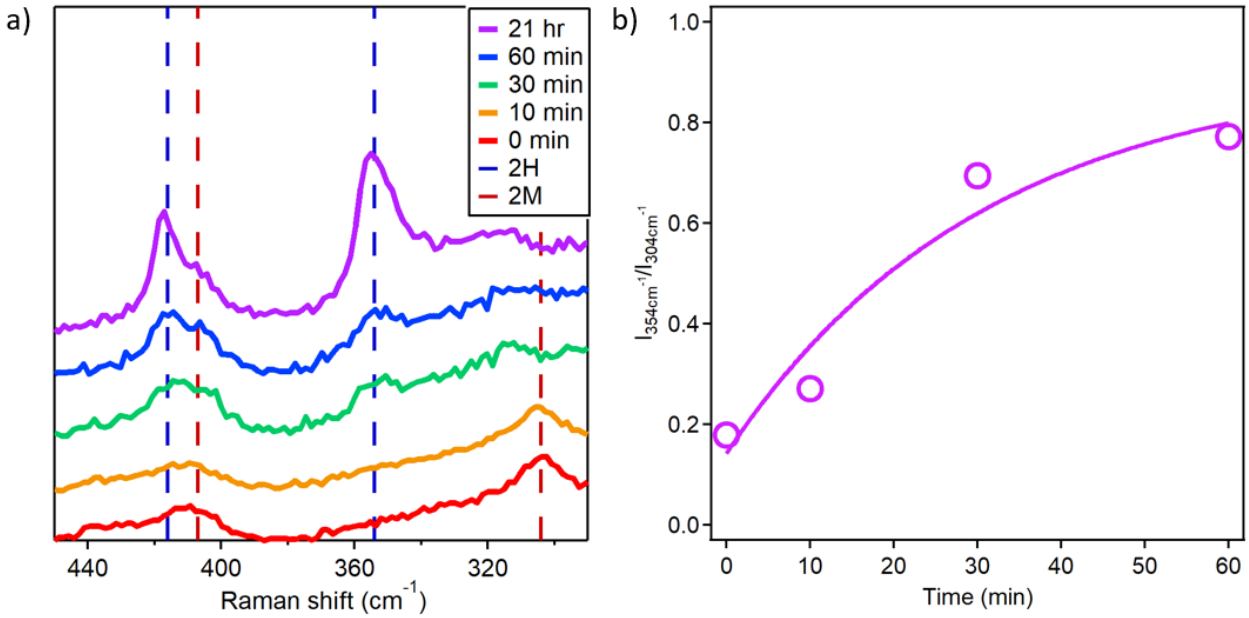

Figure 2: Raman Spectra and Intensity Ratios over Time. a) Raman spectra from colloidally synthesized WS_2 NCs using 2 eq of OA to $W(CO)_6$ with Bn_2S_2 via one-pot method reacting at 330°C for various times. b) Intensity ratios of the 2H/2M Raman modes as a function of time.

These results show that during the formation of WS_2 NCs, they first nucleate as the 2M phase. Then, over time, they gradually convert to the 2H phase. This indicates that the 2H phase cannot be accessed directly and instead must go through the

metastable 2M phase prior to accessing the thermodynamically favored 2H phase. This phenomenon can likely be attributed to the idea that the kinetic product, being the 2M phase, forms faster due to its lower energy barrier. However, by holding the reaction mixture at a high temperature for a sufficient amount of time, the thermodynamically favored product, being the 2H phase, can then be formed by converting from the existing 2M phase.

The overall reactivity can then be compared in further studies based on the Raman spectra revealing to what extent the resultant NCs have converted from the 2M to the 2H phase. For example, predominantly 2H phase NCs would imply a faster reaction rate due to its rapid conversion to the 2H phase, whereas predominantly 2M phase NCs would imply the opposite, assuming both sets of NCs were allowed to react for the same amount of time. Thus, analysis of the Raman spectra allows us to understand the effects of a given synthetic parameter on reactivity and how promoting or preventing it can allow us to access one phase over the other.

Chapter 4: Hindrance of OA on Tungsten Reactivity

Ligands are often used in colloidal syntheses to alter the reactivity and subsequently tune the phase of resultant NCs. OA in particular has been suggested to be capable of interacting with and lowering the reactivity of the tungsten precursor in TMD syntheses and subsequently hindering phase conversion.[32, 36] Here we seek to examine this further in tungsten disulfide by not only analyzing the effects of added OA on the rate of phase conversion, but also speculating on what the interaction between OA and tungsten might look like. We anticipate that as more OA ligands are present relative to tungsten, the reactivity of tungsten will be hindered. Additionally, we propose the formation of a trinuclear tungsten species based on the heated reaction of OA and tungsten hexacarbonyl. This species thus has a reduced reactivity compared to tungsten hexacarbonyl, resulting in a decreased rate of phase-conversion as well.

To do this, we performed reactions with increasing equivalents of OA relative to tungsten ranging from 0 to 100 eq and then analyzing via Raman spectroscopy. The remainder of the organic solvent is TOPO, whose quantity is adjusted in order to maintain a constant total number of moles of solvent ligands across all syntheses. In this way, a comparison of increasing amounts of OA with respect to tungsten can be made. Based on the Raman spectra in Figure 3a, the reaction where the OA to $W(CO)_6$ ratio was 100 formed NCs that exhibit primarily peaks characteristic of 2M phase tungsten disulfide, with minimal contribution from the 2H phase. Meanwhile, in the reaction in which the OA to $W(CO)_6$ ratio was decreased to 0, only peaks attributed to 2H phase WS_2 are present. The intermediate ratio of 2 eq exhibits a mixture of both the 2H and 2M phases. This can

also be visualized from Figure 3b, which shows the intensity ratios of the 2H/2M peaks with respect to equivalents of OA to $W(CO)_6$. Overall, these Raman spectra match our hypothesis that increasing the amount of OA does in fact play a role by reducing the rate of phase-conversion from the 2M to the 2H-phase.

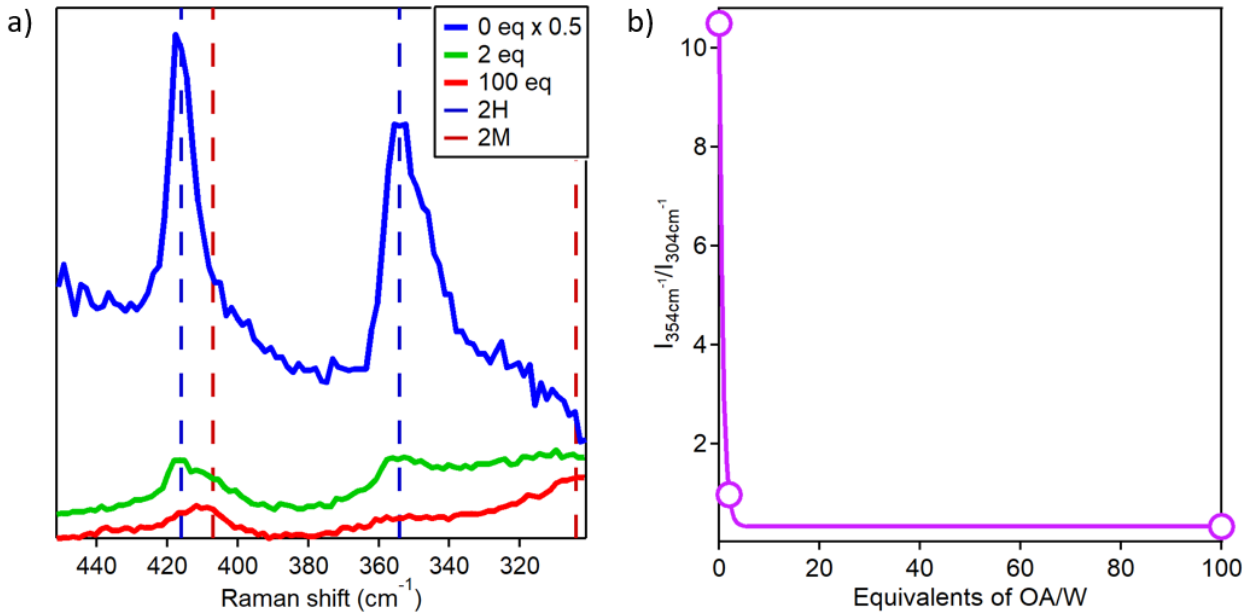

Figure 3: Raman Spectra and Intensity Ratios of OA/$W(CO)_6$ Equivalents. a) Raman spectra from colloidally synthesized WS_2 NCs using 0, 2, and 100 eq of OA/$W(CO)_6$ with octanethiol via one-pot method reacting at 300°C for 60 min. b) Intensity ratios of 2H/2M peaks for various times based on Raman spectra.

To understand the role of OA, we hypothesize that OA is able to react with tungsten to form a tungsten–oxo cluster, or other low-reactivity intermediate, upon heating. Bino et al. have shown that refluxing carboxylic acids with tungsten hexacarbonyl forms a trinuclear cluster.[38] This tungsten cluster, shown in Figure 4, is expected to react more slowly with the sulfur precursor compared to tungsten hexacarbonyl and subsequently has a reduced rate of phase conversion. This is in agreement with studies suggesting that OA is able to hinder the tungsten precursor reactivity by forming a complex with it

during heating, allowing formation of the metastable phase of tungsten dichalcogenide NCs.[32, 36] Thus, as more OA is present to react with tungsten upon heating, resulting in a less-reactive intermediate, the overall reaction-rate decreases as well as the rate of conversion from the 2M to the 2H phase.

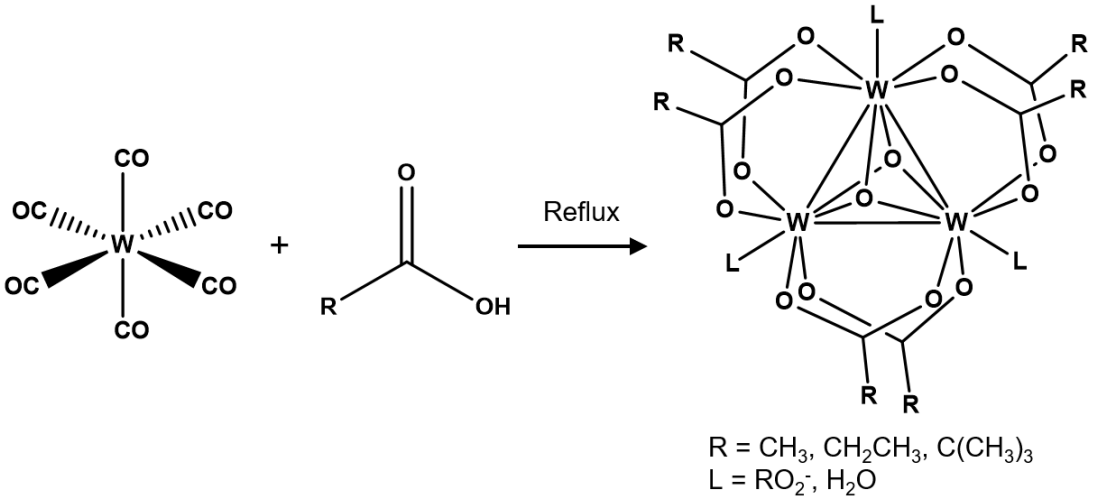

Figure 4: Trinuclear Tungsten Cluster. Schematic depicting the formation of a trinuclear tungsten cluster by refluxing tungsten hexacarbonyl with carboxylic acid.

Chapter 5: Effects of Sulfur Addition Method

Previously, we recognized the role of OA in forming a trinuclear tungsten cluster that has a comparatively a lower reactivity to that of $W(CO)_6$, which ultimately results in a decrease in phase-conversion. We then wondered whether the presence of other synthetic reagents during heating may alter the formation of the trinuclear tungsten species. If so, this could allow us to alter the formation of the trinuclear tungsten species and subsequently tune the amounts of the more and less reactive tungsten species, thus offering control over the reactivity and rate of phase conversion. A similar study has been done using hexamethyldisilazane (HMDS) to competitively interact with OA, which then leaves little to no OA to interact with the W precursor.[36] This effectively halts formation of the tungsten species with reduced reactivity and allows phase-conversion to proceed normally without any reduction from the presence of OA.

Here, we seek to understand whether the trinuclear tungsten cluster formation between OA and $W(CO)_6$ could be affected by the presence of the sulfur precursor during synthesis. We suspect that its presence during the heating process will play a role in preventing formation of the trinuclear tungsten species, allowing phase-conversion to proceed normally without hindrance from the less reactive tungsten species. To do this, the timing of the sulfur addition, being either before or after heating to the desired reaction temperature, was analyzed. In colloidal syntheses of nanocrystals, the chalcogen precursor is typically either injected into the reaction mixture once it has been heated to the target temperature (hot-injection method), or it is already included in the reaction mixture prior to heating (one-pot method). Thus, we compared the two chalcogen addition

methods for synthesizing WS_2 NCs in the following experiments in order to determine its effects on the trinuclear tungsten cluster formation and phase conversion.

We first used octanethiol as the sulfur precursor, which was added either before or after heating to the target temperature of 330°C into a mixture of $W(CO)_6$ and TOPO. Based on the Raman spectra in Figure 5a, the hot-injection method allowed for the formation of primarily 2M phase WS_2 nanocrystals after 10 minutes from the time of injection. The 2M phase converted to 2H phase at a very slow rate, with the 2M phase peak at around 305 cm^{-1} persisting even after 19 hours, at which point the nanocrystals appear to be an even mix of both 2M and 2H phase. On the other hand, Figure 5b shows that using a one pot method with octanethiol formed WS_2 nanocrystals that were already a mix of 2M and 2H phase at 10 minutes starting from the time that the reaction mixture reached the same target temperature. The NCs were nearly fully converted to 2H phase after just 30 minutes and fully converted to the 2H phase after 21 hours.

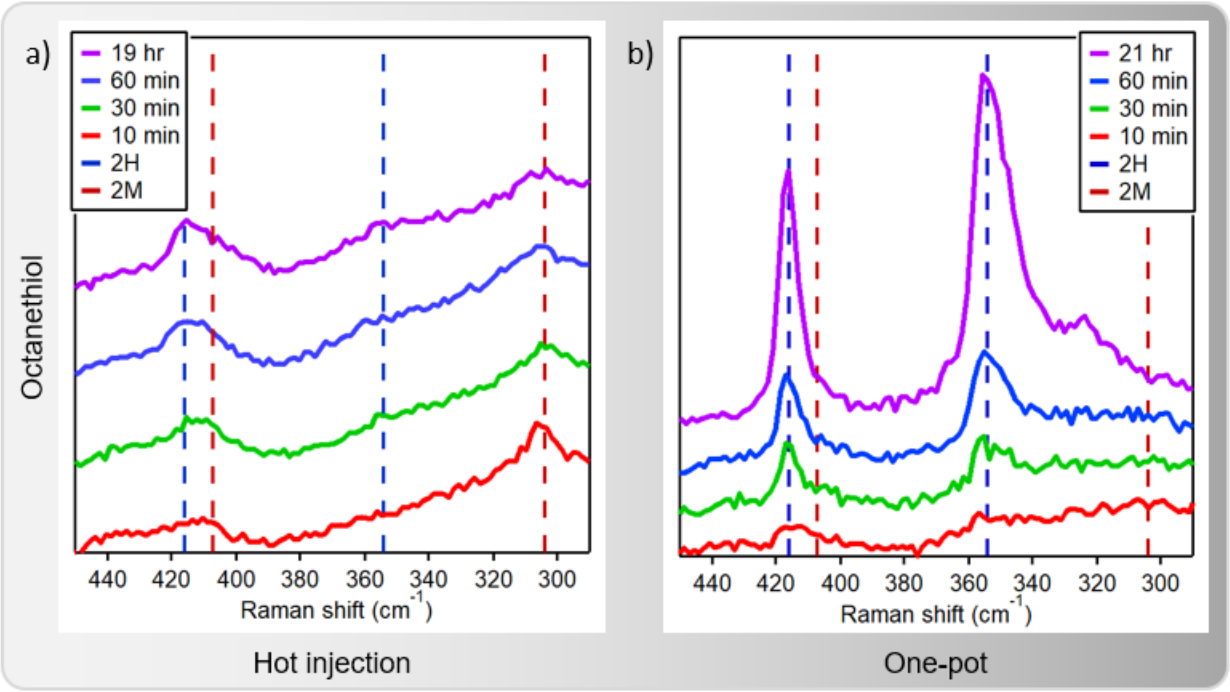

Figure 5: Raman Spectra of Octanethiol via One-pot/Hot injection. Raman spectra from colloidally synthesized WS_2 NCs using 2 eq of OA to $W(CO)_6$ with octanethiol via (a) hot-injection and (b) one-pot methods at 330°C for various times.

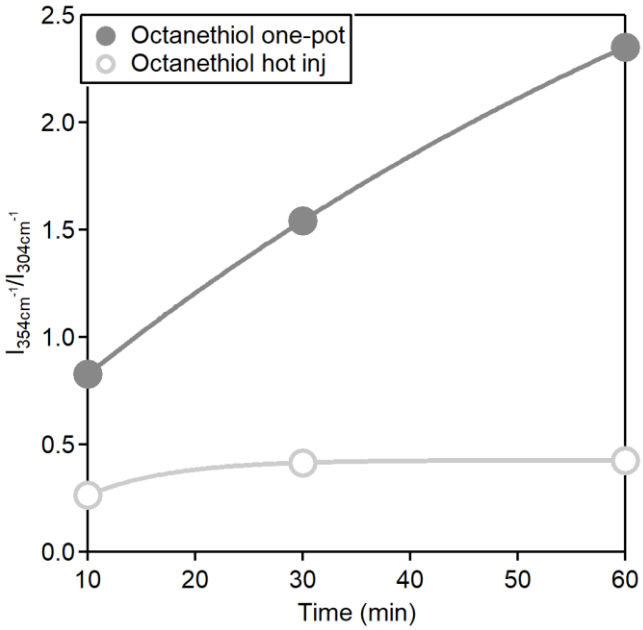

Figure 6: Intensity Ratios of Octanethiol via One-pot/Hot injection. Intensity ratios of 2H/2M peaks for various times based on Raman spectra from colloidally synthesized WS_2 NCs using 2 eq of OA/$W(CO)_6$ with dibenzyl disulfide via one-pot/hot injection method reacting at 330°C.

It was noted that the reaction mixture for the one pot method turned opaque black at around 280°C, whereas the reaction mixture for the hot-injection method remained colorless up until the tungsten precursor was injected. The opaque black color is indicative of the presence of NCs. This implies that the NC formation in the one pot method begins before reaching the target temperature, whereas the NC formation in the hot-injection method begins at the time of injection. It is difficult, however, to determine exactly at what temperature the nanocrystal formation process begins in the one pot method, so for comparison the heat-up time from 100°C to 330°C was recorded at 5 minutes. Therefore, the total NC formation time of the one pot, 10-minute aliquot for example would be somewhere between 10 and 15 minutes, which is more time compared to the hot-injection, 10-minute aliquot at exactly 10 minutes. Thus, the early timed aliquots for the one pot and hot-injection method should not directly be compared to each other to determine the rate of nanocrystal-phase conversion. That being said, overall, the one-pot method reaction underwent phase conversion to 2H phase WS_2 at a faster rate comparatively, even when accounting for the difference of up to 5 minutes between the two heat-up method reactions.

To understand the difference in phase-conversion between the hot-injection and one-pot method, we considered their differences. During the hot-injection method, tungsten hexacarbonyl is heated to high temperatures, which would allow time for some of the OA ligands to interact with the tungsten to form the trinuclear tungsten cluster species. Then when the sulfur precursor is added via hot-injection upon reaching the target temperature, it is primarily reacting with the less reactive trinuclear tungsten species. This results in the slow phase-conversion from the hot-injection method, as

shown in Figure 7. During the one-pot method, however, the sulfur precursor is already in solution prior to heating and is present to compete with OA for interaction with the tungsten upon heating. This does not allow as many OA ligands to form the trinuclear tungsten species, which has a lower reactivity than the original tungsten hexacarbonyl species. With predominantly $W(CO)_6$ reacting with the sulfur precursor in the one-pot method, the rate of phase-conversion is comparatively faster.

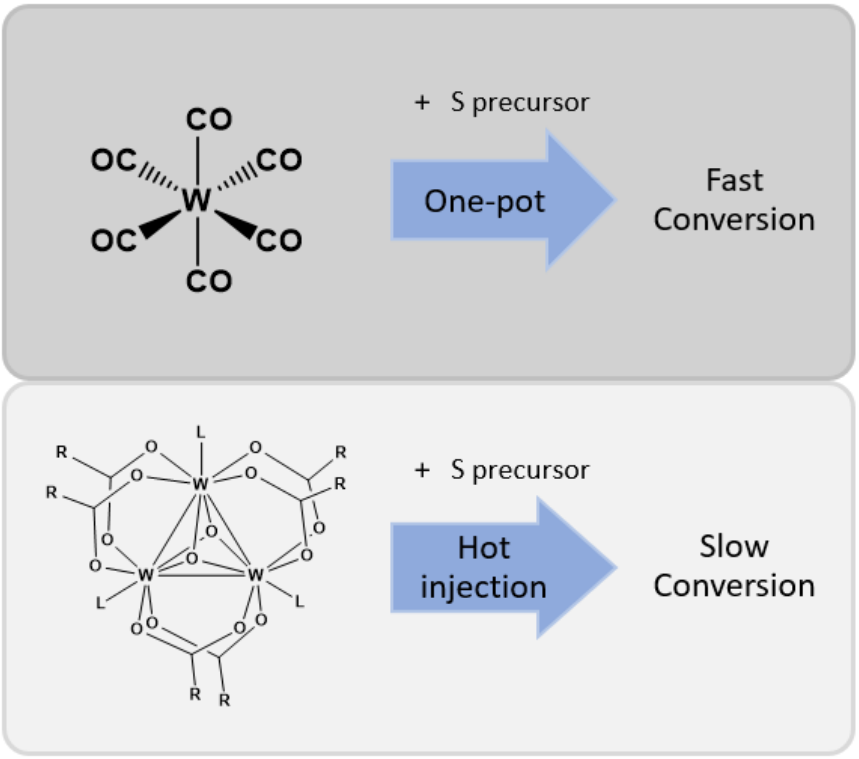

Figure 7: Chalcogen Addition Method. Schematic shown to illustrate that when using the one-pot method, the S precursor is primarily reacting with $W(CO)_6$, resulting in rapid phase-conversion. When using the hot injection method, however, the S precursor primarily reacts with the less reactive trinuclear tungsten cluster species, resulting in slow phase-conversion.

Chapter 6: Enhanced Phase-conversion with Thiols

Previously, we obtained the promising result that the one-pot chalcogen addition method yields rapid phase-conversion by allowing the sulfur precursor to primarily react with $W(CO)_6$. On the other hand, the hot-injection method yields slower phase-conversion by promoting formation of the less reactive trinuclear tungsten species, with which the sulfur precursor primarily reacts. We then sought to understand whether this difference in phase-conversion via chalcogen addition method is applicable to all sulfur precursors, as this would then be a more broadly useful synthetic tool for tuning the phase. Alternatively, this approach may be more specific to thiols, in which case our goal would be to understand why this was the case, and if more thiols could then lead to an even faster rate of phase-conversion. We suspect that in addition to what we have already discussed, the thiol is in some way playing a role to further increase the phase-conversion.

To test this, we first sought to find a non-thiol sulfur precursor with similar reactivity to octanethiol to use in a comparison test, the results of which are shown in the Raman spectra in Appendix A. Diphenyl disulfide and n-octyl sulfide were also tested but did not produce any NCs detectable by Raman and were therefore not included in the spectra. It was determined that dibenzyl disulfide would be most suitable based on its similar rate of phase-conversion to octanethiol. We then performed analogous experiments of both chalcogen addition methods using dibenzyl disulfide in place of octanethiol and compared the results.

We first compare the two sulfur precursors using the hot-injection method. Based on the Raman spectra in Figure 8a, the 2M peak in the dibenzyl disulfide reaction at

around 304 cm^{-1} showed reduced intensity by 30 minutes, whereas that same peak in the octanethiol reaction persisted at a comparatively higher intensity. Additionally, the 2H peak in the dibenzyl disulfide reaction at around 354 cm^{-1} started to grow in by 30 minutes, whereas that same peak in the octanethiol reaction was barely detectable after 19 hours. This suggests that with the hot-injection method, the NCs synthesized using dibenzyl disulfide showed somewhat faster phase conversion compared to the NCs synthesized using octanethiol, which can be seen in Figure 9 from the intensity ratios of 2H/2M peaks based on the Raman spectra.

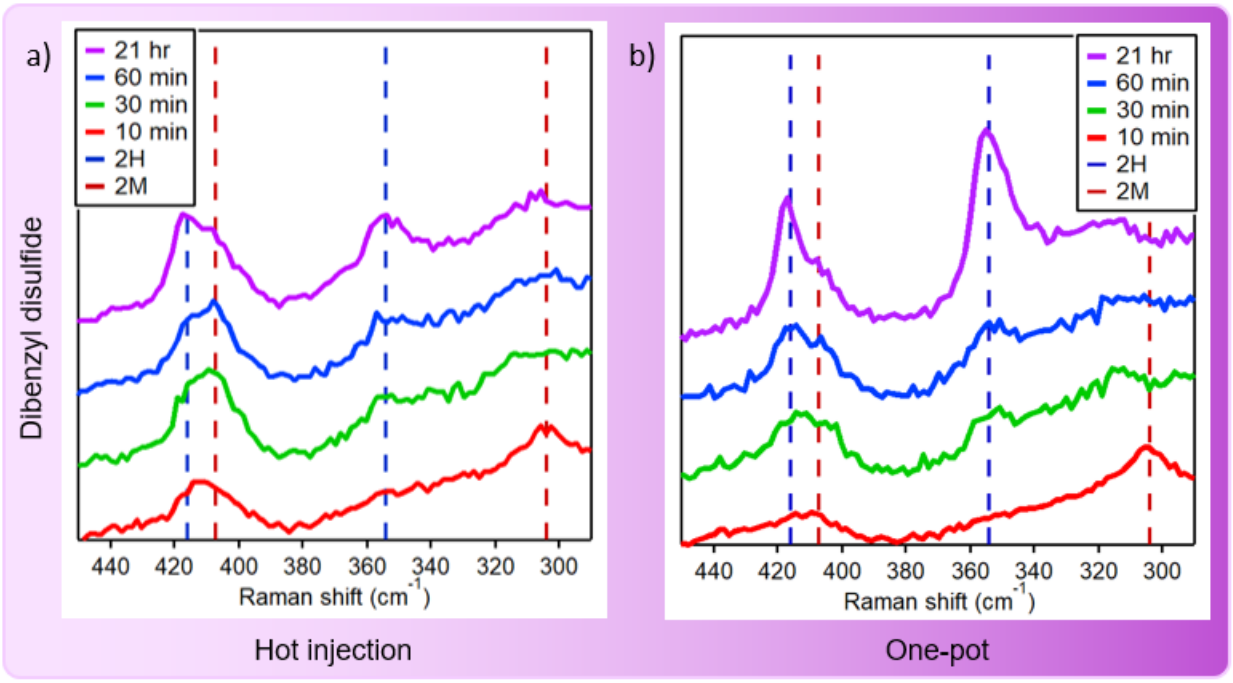

Figure 8: Raman Spectra of Bn_2S_2 via One-pot/Hot injection. Raman spectra from colloidally synthesized WS_2 NCs using 2 eq of OA to $W(CO)_6$ with dibenzyl disulfide via (a) hot-injection and (b) one-pot methods at 330°C for various times.

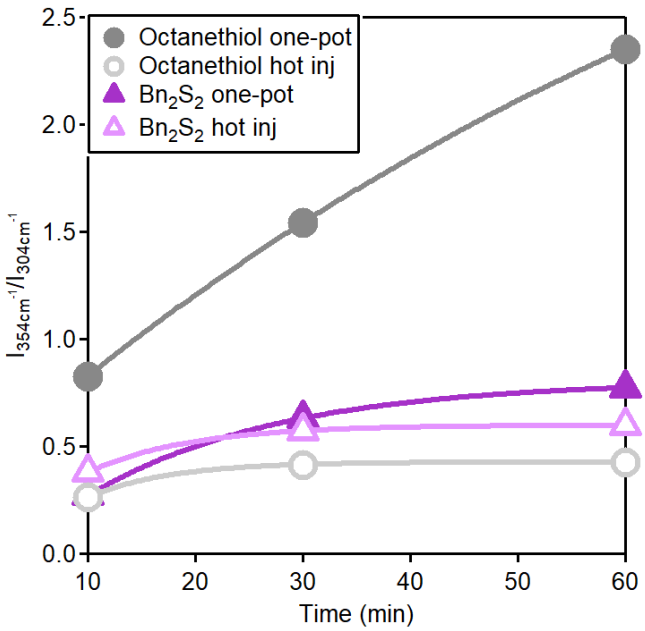

Figure 9: Intensity Ratios of Octanethiol/Bn_2S_2 via One-pot/Hot injection. Intensity ratios of 2H/2M peaks for various times based on Raman spectra from colloidally synthesized WS_2 NCs using 2 eq of OA/$W(CO)_6$ with octanethiol/dibenzyl disulfide via one-pot/hot injection method reacting at 330°C.

The difference between the two sulfur precursors using the hot-injection method could be attributed to their difference in C–S bond dissociation energy (BDE), which has been shown to play a role in tuning the phase of colloidally synthesized metal sulfide NCs.[28] Specifically, a link has been found between sulfur precursors with low C–S BDEs having high reactivity, which in our case would result in faster phase conversion. For dibenzyl disulfide, the C–S BDE had been calculated to be 50.2 kcal/mol.[28] For octanethiol, the C–S BDE was approximated at 74.1 kcal/mol based on the calculated value for hexanethiol, given that additional carbons make little impact on the C–S BDE of long-chain alkanethiols.[39] Since dibenzyl disulfide has a lower C–S BDE, it would then dissociate more readily compared to octanethiol and subsequently react and undergo phase-conversion at a faster rate.

Despite dibenzyl disulfide contributing to faster phase conversion compared to octanethiol via the hot-injection method of chalcogen addition, the opposite is true for the one-pot method. Based on the Raman spectra in Figure 8b, the dibenzyl disulfide reaction showed a fairly strong 2M peak at around 304 cm^{-1} at 10 minutes, while that same peak in the octanethiol reaction is already barely detectable. At 60 minutes, the dibenzyl disulfide reaction still showed a significant contribution from the 2M phase based on the peak at around 407 cm^{-1}, which is still present even after being left to react overnight. However, by just 30 minutes, that same peak is also barely detectable in the octanethiol reaction, indicating nearly full conversion at a considerably faster rate.

While the dibenzyl disulfide reactions do show somewhat faster phase-conversion in the one-pot method of chalcogen addition compared to the hot-injection method, octanethiol shows a much more drastic increase in phase-conversion. This can be clearly seen from the intensity ratios in Figure 9 as well. To explain this discrepancy, we suspect that the thiol in particular may be assisting in the drastic increase in phase conversion. To confirm that this phenomenon is in fact specific to thiols, we ran a third comparison test using dodecanethiol (DDT). As indicated in Appendix B, DDT displayed similarly rapid phase conversion to that of octanethiol in the one-pot compared to the hot injection method.

Based on these results, we propose that thiols promote rapid phase-conversion by increasing the distance between layers. This increase is likely due to the inclusion of the alkyl group as a "crystal-bound" ligand, which maintains the alkyl group.[40] This phenomenon, conceptualized by Turo & Macdonald,[41] suggests that thiols can act as capping ligands by sitting in high coordination sites and becoming the terminal S layer of

the NC. This effectively increases accessibility to undergo further reaction and ultimately promotes more rapid phase conversion from the 2M to the 2H phase based on the use of thiols as the sulfur precursor. On the other hand, diorganodisulfide precursors likely react via a different mechanism that does not maintain the alkyl group, resulting in no expansion of the layers.

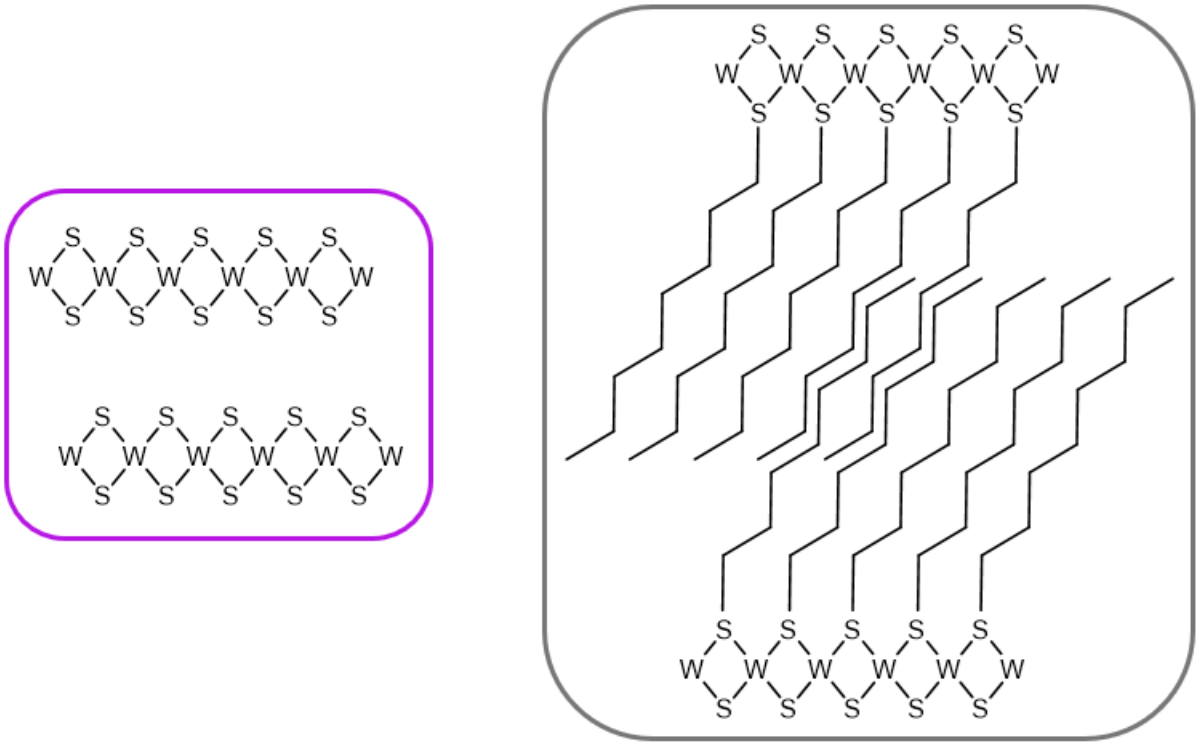

Figure 10: Schematic of Lattice Expansion. Crystal-bound thiols retain R groups, which effectively expands the lattice and reduces steric effects, promoting phase conversion.

Based on the idea that the expanded lattice caused by thiols is what promotes increased phase conversion in the synthesis of WS_2 NCs, we further speculate what relative amount of thiol added would maximize rapid phase-conversion. Specifically, our goal is to experimentally determine the effects of increased thiol to tungsten ratios on the rate of phase conversion. This would tell us how much thiol is required to allow for the

largest interlayer distance, meaning that each sulfur on the lattice surface retains a fully-extended R group with little to no defects. This would then maximize lattice expansion as well as the rate of phase-conversion. Thus, we suspect that increasing the thiol to tungsten ratio would also increase phase-conversion to a certain extent, at which point the interlayer distance would reach a maximum and subsequently no further addition of thiol would increase phase-conversion. To test this, we ran a series of WS_2 reactions using increasing molar ratios of thiol to tungsten hexacarbonyl starting at 2-to-1, the lowest being the minimum stoichiometric ratio necessary for tungsten disulfide formation. To prevent any additional influences, we excluded OA from the solvent mixture for this series of reactions.

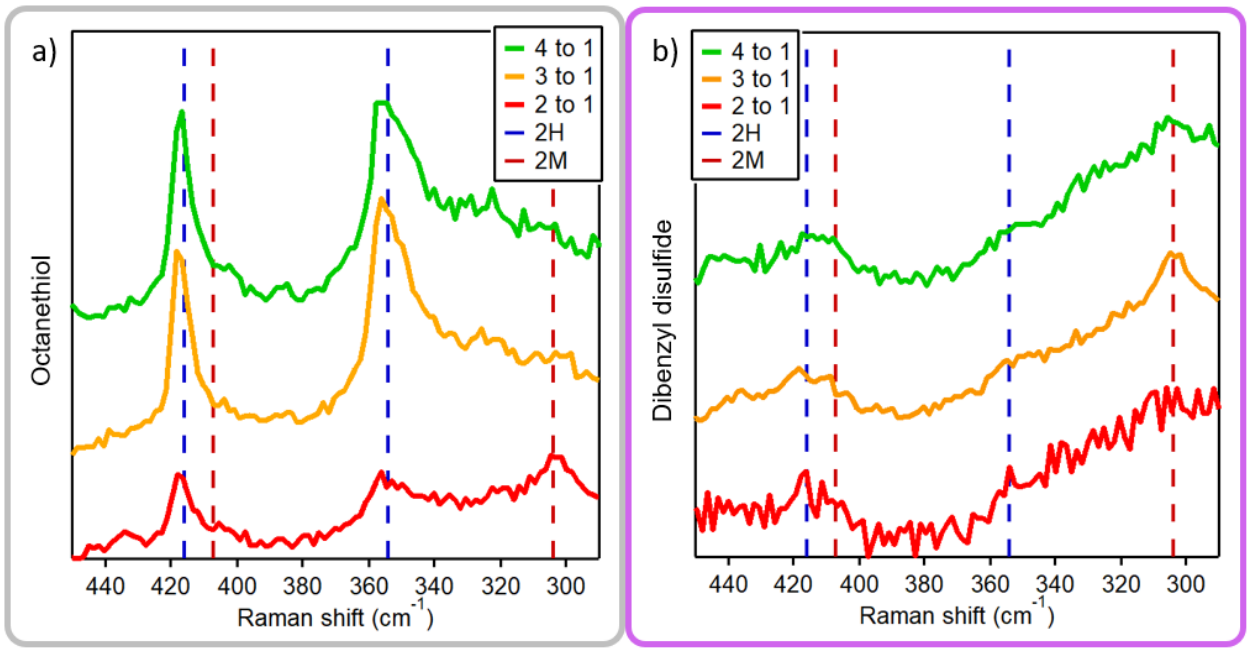

Figure 12: Raman Spectra using Ratios of Octanethiol/Bn_2S_2 to $W(CO)_6$. Raman spectra of colloidally synthesized WS_2 NCs using various ratios of a) octanethiol and b) dibenzyl disulfide to $W(CO)_6$ via one-pot method reacting at 300°C for 60 min.

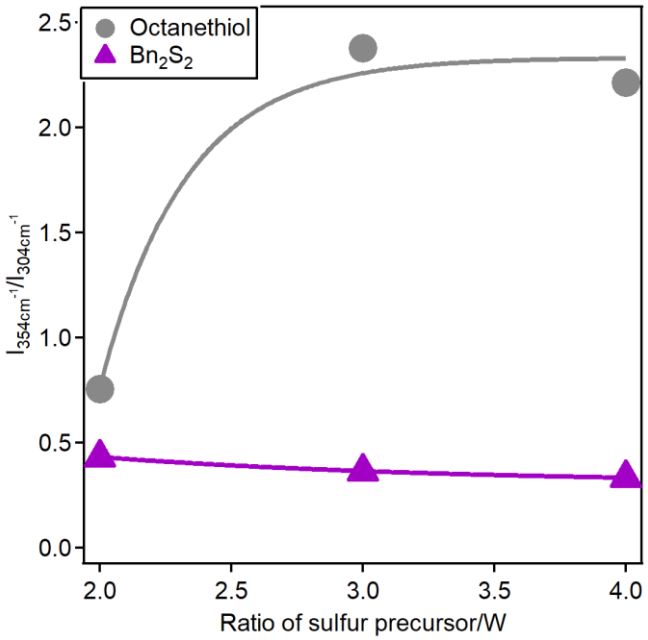

Figure 13: Intensity Ratios for Ratios of Octanethiol/Bn_2S_2 to $W(CO)_6$. Intensity ratios of 2H/2M peaks from Raman spectra of colloidally synthesized WS_2 NCs using various ratios of octanethiol and dibenzyl disulfide to $W(CO)_6$ via one-pot method reacting at 300°C for 60 min.

Based on the Raman spectra and corresponding intensity ratios of the 2H/2M peaks in Figure 12a and Figure 13 from the reactions using octanethiol, the 2-to-1 ratio showed a significant amount of 2M phase mixed with the 2H phase, indicating a somewhat slow rate of conversion at the lowest ratio. Next was the 3-to-1 ratio, which displayed peaks attributed to the 2H phase with no noticeable contribution from the 2M phase. The Raman spectra of the 4-to-1 ratio was also dominated by the 2H phase, yielding nearly identical results compared to the 3-to-1. Overall, the data suggests that increasing the thiol to tungsten ratio can cause an increase in the rate of phase conversion from 2M to 2H. However, when the maximum ratio of 3-to-1 is achieved, further addition of thiol has no effect. This indicates that a small excess of thiol beyond the stoichiometric ratio for WS_2 is optimal for allowing the R groups of the thiols embedded in the surface of

the lattice to be fully extended with little to no defects and subsequently maximize the interlayer distance, as depicted in Figure 10. Any less would likely result in defects resulting from some thiols not retaining their R group and being fully extended. The data also confirms that adding more thiols beyond the optimal 3-to-1 ratio would lead to no additional expansion of the lattice, as the R groups of the thiols are already fully extended to maximize the interlayer distance. This results in no further increase in phase conversion, which is seen in the 4-to-1 ratio.

Previously, we determined that sulfur precursors such as dibenzyl disulfide are unable to promote rapid phase conversion due to the loss of their R group during synthesis, making them unable to expand the lattice. It was then expected that increasing the ratio of dibenzyl disulfide, for example, relative to tungsten would have no effect on the phase conversion. As a proof-of-concept test, we ran an analogous experiment using dibenzyl disulfide in place of octanethiol. This indeed showed by Raman in Figure 12b and Figure 13 that phase conversion remains largely unaffected by the ratio of a short-chain sulfur precursor relative to tungsten hexacarbonyl, confirming our hypothesis.

In conclusion, the metastable 2M phase can be accessed by utilizing OA in order to promote formation of the trinuclear tungsten cluster, which has reduced reactivity compared to tungsten hexacarbonyl and subsequently reduces the possibility of phase conversion. This should be done in conjunction with the hot-injection method, since the one-pot method will hinder formation of the trinuclear tungsten cluster and result in phase-conversion to the 2H-phase. On the other hand, accessing the 2H phase can be achieved using the one-pot method in conjunction with thiol sulfur precursors. This is due to the

rapid phase-conversion caused by thiols embedding themselves into the lattice surface during heating and increasing the interlayer distance with their sterically bulky R groups. The expanded lattice then allows more accessibility for further rearrangement and subsequently promotes phase-conversion to the 2H phase. Utilizing a small excess of thiol beyond the 2-to-1 stoichiometric ratio for WS_2 should also be used to prevent defects and allow the R groups of the crystal-bound thiols to be fully extended in order to maximize the interlayer distance. Phase-conversion via lattice expansion can also be avoided by using sulfur precursors such as dibenzyl disulfide, as these molecules lose their R groups during synthesis and are thus incapable of increasing the interlayer distance.

Material from various chapters, namely Chapter 6, in part are currently being prepared for submission for publication. Ms. Tamura will be the third author on this paper. Geisenhoff, J. Q.*; Yin, H.*; Tamura, A. K.; Schimpf, A. M. Crystal-bound thiols for the interlayer expansion of tungsten and molybdenum disulfide nanocrystals. In preparation. *These authors contributed equally.

APPENDIX

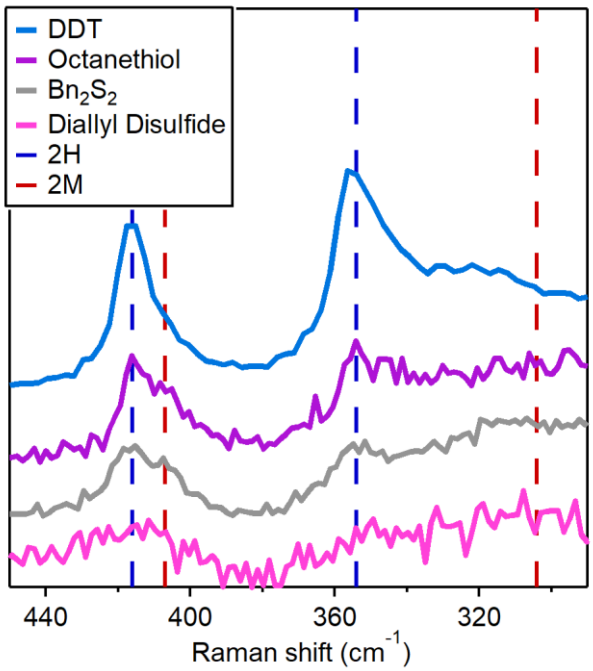

Appendix A: Raman Spectra of Sulfur Precursors. Raman spectra from colloidally synthesized WS_2 NCs using 2 eq of $OA/W(CO)_6$ with DDT, octanethiol, Bn_2S_2 and diallyl disulfide reacting at 300°C for 60 min.

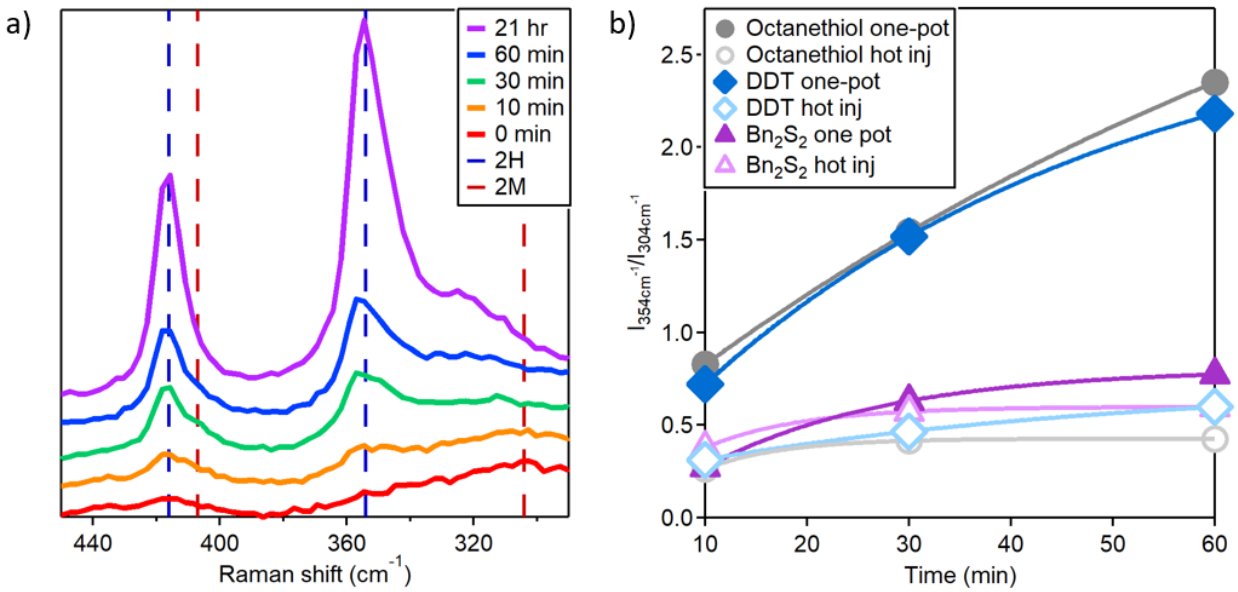

Appendix B: Raman Spectra and Intensity Ratios of DDT Comparison. a) Raman spectra from colloidally synthesized WS_2 NCs using 2 eq of OA to $W(CO)_6$ with DDT via one-pot method at 330°C for various times. b) Intensity ratios of 2H/2M peaks based on Raman spectra for analogous reactions using octanethiol, DDT, and Bn_2S_2 via one-pot/hot injection methods.

REFERENCES

1. Novoselov, K. S.; Geim, A. K.; Morozov, S. V.; Jiang, D.; Zhang, Y.; Dubonos, S. V.; Grigorieva, I. V.; Firsov, A. A., Electric Field Effect in Atomically Thin Carbon Films. *Science* **2004,** *306*, 666-69.

2. Yin, Z.; Zhu, J.; He, Q.; Cao, D.; Tan, C.; Chen, H.; Yan, Q.; Zhang, H., Graphene-Based Materials for Solar Cell Applications. *Adv Energy Mater* **2014,** *4*, 1300574.

3. Huang, H.; Yin, Z.; Wu, S.; Qi, X.; He, Q.; Zhang, Q.; Yan, Q.; Boey, F.; Zhang, H., Graphene-Based Materials: Synthesis, Characterization, Properties, and Applications. *Small* **2011,** *7* (14), 1876-1902.

4. Sun, Y.; Terrones, M.; Schaak, R. E., Colloidal Nanostructures of Transition-Metal Dichalcogenides. *Acc Chem Res* **2021,** *54*, 1517-1527.

5. Manzeli, S.; Ovchinnikov, D.; Pasquier, D.; Yazyev, O. V.; Kis, A., 2D transition metal dichalcogenides. *Nat Rev Mater* **2017,** *2*, 17033.

6. Chhowalla, M.; Shin, H. S.; Eda, G.; Li, L.; Loh, K. P.; Zhang, H., The chemistry of two-dimensional layered transition metal dichalcogenide nanosheets. *Nat Chem* **2013,** *5*, 263-75.

7. Wang, Q. H.; Kalantar-Zadeh, K.; Kis, A.; Coleman, J. N.; Strano, M. S., Electronics and optoelectronics of two-dimensional transition metal dichalcogenides. *Nat Nanotechnol* **2012,** *7*, 699-712.

8. Sokolikova, M. S.; Mattevi, C., Direct synthesis of metastable phases of 2D transition metal dichalcogenides. *Chem Soc Rev* **2020,** *49*, 3952-80.

9. Choe, D.; Sung, H.; Chang, K. J., Understanding topological phase transition in monolayer transition metal dichalcogenides. *Phys Rev B* **2016,** *93*, 125109.

10. Fang, Y.; Pan, J.; Zhang, D.; Wang, D.; Hirose, H. T.; Terashima, T.; Uji, S.; Yuan, Y.; Li, W.; Tian, Z.; Xue, J.; Ma, Y.; Zhao, W.; Xue, Q.; Mu, G.; Zhang, H.; Huang, F., Discovery of Superconductivity in 2M WS2 with Possible Topological Surface States. *Adv Mater* **2019,** *31* (30), 1901942.

11. Suzuki, R.; Sakano, M.; Zhang, Y. J.; Akashi, R.; Morikawa, D.; Harasawa, A.; Yaji, K.; Kuroda, K.; Miyamoto, K.; Okuda, T.; Ishizaka, K.; Arita, R.; Iwasa, Y., Valley-dependent spin polarization in bulk MoS2 with broken inversion symmetry. *Nat Nanotechnol* **2014,** *9*, 611-17.

12. Zeng, Z.; Sun, X.; Zhang, D.; Zheng, W.; Fan, X.; He, M.; Xu, T.; Sun, L.; Wang, X.; Pan, A., Controlled Vapor Growth and Nonlinear Optical Applications of Large-Area 3R Phase WS2 and WSe2 Atomic Layers. *Adv Funct Mater* **2019,** *29*, 1806874.

13. Ovchinnikov, D.; Allain, A.; Huang, Y.; Dumcenco, D.; Kis, A., Electrical Transport Properties of Single-Layer WS2. *Acs Nano* **2014,** *8* (8), 8174-81.

14. Georgiou, T.; Jalil, R.; Belle, B. D.; Britnell, B.; Gorbachev, R. V.; Morozov, S. V.; Kim, Y.; Gholinia, A.; Haigh, S. J.; Makarovsky, O.; Eaves, L.; Ponomarenko, L. A.; Geim, A. K.; Novoselov, K. S.; Mishchenko, A., Vertical field-effect transistor based on graphene–WS2 heterostructures for flexible and transparent electronics. *Nat Nanotechnol* **2013,** *8*, 100-3.

15. Voiry, D.; Yamaguchi, H.; Li, J.; Silva, R.; Alves, D. C. B.; Fujita, T.; Chen, M.; Asefa, T.; Shenoy, V. B.; Eda, G.; Chhowalla, M., Enhanced catalytic activity in strained chemically exfoliated WS2 nanosheets for hydrogen evolution. *Nature Materials* **2013,** *12* (9), 850-855.

16. Lukowski, M. A.; Daniel, A. S.; English, C. R.; Meng, F.; Forticaux, A.; Hamers, R. J.; Jin, S., Highly active hydrogen evolution catalysis from metallic WS2 nanosheets. *Energy & Environmental Science* **2014,** *7* (8), 2608-2613.

17. Benck, J. D.; Hellstern, T. R.; Kibsgaard, J.; Chakthranont, P.; Jaramillo, T. F., Catalyzing the Hydrogen Evolution Reaction (HER) with Molybdenum Sulfide Nanomaterials. *Acs Catal* **2014,** *4* (11), 3957-3971.

18. Benck, J. D.; Hellstern, T. R.; Kibsgaard, J.; Chakthranont, P.; Jaramillo, T. F., Catalyzing the Hydrogen Evolution Reaction (HER) with Molybdenum Sulfide Nanomaterials. *Acs Catal* **2014,** *4*, 3957-71.

19. Yang, J.; Voiry, D.; Ahn, S. J.; Kang, D.; Kim, A. Y.; Chhowalla, M.; Shin, H. S., Two-Dimensional Hybrid Nanosheets of Tungsten Disulfide and Reduced Graphene Oxide as Catalysts for Enhanced Hydrogen Evolution. *Angewandte Chemie International Edition* **2013,** *52* (51), 13751-13754.

20. Li, Y.; Wang, H.; Xie, L.; Liang, Y.; Hong, G.; Dai, H., MoS2 Nanoparticles Grown on Graphene: An Advanced Catalyst for the Hydrogen Evolution Reaction. *J Am Chem Soc* **2011,** *133* (19), 7296-99.

21. Qian, X.; Liu, J.; Fu, L.; Li, J., Quantum spin Hall effect in two-dimensional transition metal dichalcogenides. *Science* **2014,** *346* (6215), 1344-1347.

22. Xiao, D.; Liu, G.; Feng, W.; Xu, X.; Yao, W., Coupled Spin and Valley Physics in Monolayers of MoS2 and Other Group-VI Dichalcogenides. *Phys Rev Lett* **2012,** *108*, 196802.

23. Pulkin, A.; Yazyev, O. V., Spin- and valley-polarized transport across line defects in monolayer MoS2. *Phys Rev B* **2016,** *93*, 041419.

24. Zhang, X.; Cheng, H.; Zhang, H., Recent Progress in the Preparation, Assembly, Transformation, and Applications of Layer-Structured Nanodisks beyond Graphene. *Advanced Materials* **2017,** *29* (35), 1701704.

25. Bhimanapati, G. R.; Lin, Z.; Meunier, V.; Jung, Y.; Cha, J.; Das, S.; Xiao, D.; Son, Y.; Strano, M. S.; Cooper, V. R.; Liang, L.; Louie, S. G.; Ringe, E.; Zhou, W.; Kim, S. S.; Naik, R. R.; Sumpter, B. G.; Terrones, H.; Xia, F.; Wang, Y.; Zhu, J.; Akinwande, D.; Alem, N.; Schuller, J. A.; Schaak, R. E.; Terrones, M.; Robinson, J. A., Recent Advances in Two-Dimensional Materials beyond Graphene. *ACS Nano* **2015,** *9* (12), 11509-11539.

26. Han, J. H.; Kwak, M.; Kim, Y.; Cheon, J., Recent Advances in the Solution-Based Preparation of Two-Dimensional Layered Transition Metal Chalcogenide Nanostructures. *Chemical Reviews* **2018,** *118* (13), 6151-6188.

27. LaMer, V. K.; Dinegar, R. H., Theory, Production and Mechanism of Formation of Monodispersed Hydrosols. *J Am Chem Soc* **1950,** *72* (11), 4847-54.

28. Rhodes, J. M.; Jones, C. A.; Thal, L. B.; Macdonald, J. E., Phase-Controlled Colloidal Syntheses of Iron Sulfide Nanocrystals via Sulfur Precursor Reactivity and Direct Pyrite Precipitation. *Chem Mater* **2017,** *29*, 8521-30.

29. Ruan, L.; Shen, W.; Wang, A.; Xiang, A.; Deng, Z., Alkyl-Thiol Ligand-Induced Shape- and Crystalline Phase-Controlled Synthesis of Stable Perovskite-Related CsPb2Br5 Nanocrystals at Room Temperature. *J Phys Chem Lett* **2017,** *8*, 3853-60.

30. Barim, G.; Smock, S. R.; Antunez, P. D.; Glaser, D.; Brutchey, R. L., Phase control in the colloidal synthesis of well-defined nickel sulfide nanocrystals. *Nanoscale* **2018,** *10*, 16298-306.

31. Tappan, B. A.; Horton, M. K.; Brutchey, R. L., Ligand-Mediated Phase Control in Colloidal AgInSe2 Nanocrystals. *Chem Mater* **2020,** *32*, 2935-45.

32. Geisenhoff, J. Q.; Tamura, A. K.; Schimpf, A. M., Using ligands to control reactivity, size and phase in the colloidal synthesis of WSe2 nanocrystals. *Chem Commun* **2019,** *55* (60), 8856-59.

33. Chen, W.; Karton, A.; Hussian, T.; Javaid, S.; Wang, F.; Panga, Y.; Jia, G., Spontaneous shape and phase control of colloidal ZnSe nanocrystals by tailoring Se precursor reactivity. *CrystEngComm* **2019,** *21*, 2955.

34. Grandhi, G. K.; Viswanath, N. S. M.; Cho, H. B.; Kim, S. M.; Im, W. B., Highly stable hetero-structured green-emitting cesium lead bromide nanocrystals via ligand-mediated phase control. *Nanoscale* **2019,** *11*, 21137-46.

35. Zhou, P.; Schiettecatte, P.; Vandichel, M.; Rousaki, A.; Vandenabeele, P.; Hens, Z.; Singh, S., Synthesis of Colloidal WSe_2 Nanocrystals: Polymorphism Control by Precursor-Ligand Chemistry. *Cryst Growth Des* **2021,** *21* (3), 1451-60.

36. Mahler, B.; Hoepfner, V.; Liao, K.; Ozin, G. A., Colloidal synthesis of 1T-WS2 and 2H-WS2 nanosheets: applications for photocatalytic hydrogen evolution. *J Am Chem Soc* **2014,** *136* (40), 14121-7.

37. Liu, Z. Q.; Li, N.; Su, C.; Zhao, H. Y.; Xu, L. L.; Yin, Z. Y.; Li, J.; Du, Y. P., Colloidal synthesis of 1T ' phase dominated WS2 towards endurable electrocatalysis. *Nano Energy* **2018,** *50*, 176-181.

38. Bino, A.; Cotton, F. A.; Dori, Z.; Koch, S.; Kueppers, H.; Millar, M.; Sekutowski, J. C., A new class of trinuclear tungsten(IV) cluster compounds with tungsten-tungsten single bonds. *Inorganic Chemistry* **1978,** *17* (11), 3245-3253.

39. Shi, J.; Hu, X.; Liang, S., A Computational Study of C–S Bond Dissociation Enthalpies in Petroleum Chemistry. *Heteroat Chem* **2011,** *22* (2), 97-105.

40. Geisenhoff, J. Q.; Yin, H.; Tamura, A. K.; Schimpf, A. M., *In preparation.*

41. Turo, M. J.; Macdonald, J. E., Crystal-Bound vs Surface-Bound Thiols on Nanocrystals. *ACS Nano* **2014,** *8* (10), 10205-10213.